Published by :
http://www.ijert.org

International Journal of Engineering Research & Technology (IJERT)
ISSN: 2278-0181
Vol. 12 Issue 05, May-2023

Mm-Wave OFDM Uplink Transmission Using Sparse Frequency Selective Channel Model

Pragnya Sudipta Tripathy
Department Name: Electronics & Instrumentation Engineering
Branch: Electronics & Communication Engineering
University Name: OUTR, BBSR
State: Odisha, India

Professor Name : Bijay Kumar Ekka
Department Name: Electronics & Instrmentation Engineering
University Name: OUTR, BBSR
State: Odisha, India

Abstract - **This research paper investigates the impact of wideband and hybrid receiving on the spectral efficiency of millimeter-wave OFDM uplink transmission, specifically using a frequency selective channel with sparse formulation model. The study reveals that an increase in bandwidth can cause the beam squint effect, leading to a decrease in spectral efficiency. However, use of the Sparse Formulation of Frequency Selective Channel Model (FSCM-SF) can enhance the analysis of the system's spectral efficiency. In terms of spectral efficiency, simulation results show that FSCM-SF implementation outperforms Spatial-Frequency-Wideband implementation. Furthermore, the FSCM-SF output is more responsive than the traditional form. The study shows that, regardless of system bandwidth, the sparse formulation of the Frequency Selective Channel Model can improve the spectral efficiency of millimeter-wave OFDM uplink transmission. More research is needed to improve the system's efficiency.**

Keywords— Hybrid Receiving, OFDM, Uplink Transmission, Sparse Frequency Selective Channel Model, Beam Squint Effect, System's Spectral Efficiency, Signal-To-Noise Ratio (SNR), Bandwidth, Subcarriers.

I. INTRODUCTION

Because of its ability to transmit data at high speeds with minimal delay between transmissions, millimetre wave (mmWave) communication has a lot of potential for use in wireless communication systems. However, mmWave communication is plagued with issues such as high blockage, limited coverage, and path loss. In response to these difficulties, orthogonal frequency division multiplexing, also known as OFDM, has seen widespread application in mmWave systems. This allows for improved spectral efficiency as well as mitigation of the effects of frequency-selective fading. It has been suggested that using hybrid receiving, which combines analogue and digital processing, can be an efficient method for overcoming the limitations that are posed by conventional receivers in mmWave OFDM systems. Hybrid receiving is a technique that combines analogue beamforming and digital signal processing in order to take advantage of the high directionality of mmWave channels. Because of the reduced complexity of digital signal processing, hybrid reception is becoming more popular. In contrast, the precision of the channel state information (CSI) and the beam alignment of the transmitter and receiver determine hybrid reception performance. The wideband effects of mmWave channels can cause beam squinting, which reduces spectral efficiency significantly. This paper investigates the impact of wideband and hybrid receiving on the spectral efficiency of mmWave OFDM uplink transmission, taking into account the channel model's spatial and frequency wideband implications. To improve the precision of our research, we use a sparsely constructed Frequency Selective Channel Model and provide simulation data to back up our findings. Section II introduces the system model after an analysis of the channel model in Section III, and Section IV presents simulation results. Section IV investigates the effectiveness of the spectrum in relation to the number of subcarriers, bandwidth, and non-orthogonality of the OFDM subcarriers. We provide some summaries in the study's conclusion section.

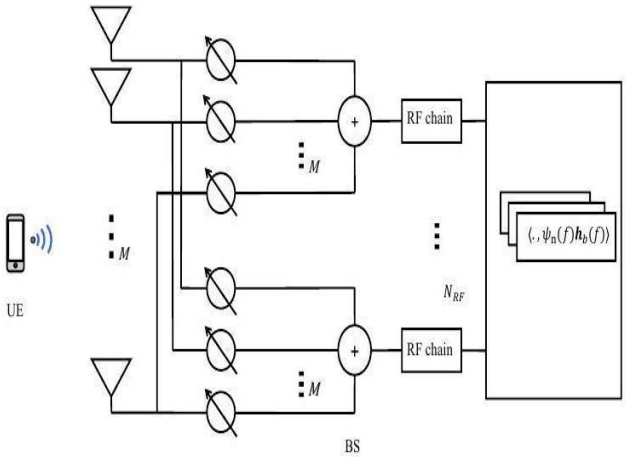

Fig. 1. mmWave uplink system

II. SYSTEM MODELLING

The decision is shown in Figure 1. In this configuration, a user equipment (UE) with an antenna transmits a signal to a base

International Journal of Engineering Research & Technology (IJERT)
ISSN: 2278-0181
Vol. 12 Issue 05, May-2023

station (BS), which receives it. M antennas are installed on the BS in a parallel linear array. Analogue reception is possible thanks to a phase-shift network connected to the BS antennas. The N_{RF} radio frequency (RF) circuits are linked to the phase shift network. The t-th time slot's base station signal is represented as

$$y(t) = x(t) * h(t) + n(t) \in C^{M\times 1} \quad (1)$$

here $x(t)$ denotes transmitted signal,
$h(t) \in C^{M\times 1}$ denotes channel among BS and UE,
$n(t) \in C^{M\times 1}$ is noise received. Since the system operates in wide bandwidth and millimeter waveband, the channel has many channels and frequencies. Considering the double broadband effect, the notation for the m-th component of the channel vector is

$$[h(t)]_m = \sum_{l=1}^{L} \alpha_l e^{-j2\pi(m-1)\theta_l} \times Wsinc\left(W(t-(m-1)\theta_l/f_c - \tau_l)\right) \quad (2)$$

The l-th path's complex path gain α_l has a complex Gaussian distribution with a zero mean and variance σ_α^2. W is the bandwidth, and τ_l is the delay in the time of the l-th path. The number of paths is represented by L, and the frequency of the carrier is represented by f_c. Because of the array's linearity, we can state that $\theta_l = d/\lambda sin\,(\phi_l)$, where ϕ_l is the l-th path's DOA (direction of arrival), λ-wavelength, and d denotes the distance among two BS antennas. The station chose a hybrid architecture using mm-wave technology and an optimized base station architecture. Analogue beamforming is applied to the received signal prior to passing through the RF chain and transitioning to digital recording. The complex path gain, which is indicated by the symbolα_l and corresponds to the lth path, is distributed according to a complex Gaussian model with a mean of zero and a variance equal to σ_α^2. Within the scope of this discussion, W stands for the bandwidth, and τ_l denotes the amount of delay in time associated with the path of the I. L is the total paths, and f_c denoting the frequency of the carrier. As we know that the array is linear, we are able to express the angle of arrival (AOA) for the l-th path, which is denoted as $\theta_l = d/\lambda sin\,(\phi_l)$.
In this situation, ϕ_l represents the DOA for the l-th path, λ represents the wavelength, and d represents the distance between adjacent BS (base station) antennas. The station has implemented a hybrid architecture, which combines mm-wave technology with an optimized base station architecture, in order to improve the overall performance of the system. Before going through the RF chain and then making the switch to digital recording, the signal that was received goes through the process of analogue beamforming.

$$[a(\bar{\theta}_n)]_m = \frac{1}{\sqrt{M}} e^{-j2\pi(m-1)\bar{\theta}_n} \quad (3)$$

Where

$$\bar{\theta}_n = \frac{1}{M}\left(n - 1 - \frac{M-1}{2}\right) \quad (4)$$

Vectors with $n = 1,2,\cdots,M$ form into $U \in C^{M\times M}$ in which

$$[U]_n = a(\bar{\theta}_n). \quad (5)$$

The system chooses N_{RF} beams, which translates to selecting N_{RF} columns of U and creating a new matrix, $U_b \in C^{M\times N_{RF}}$. It's worth noting that $U^H U = I_M, as\ well\ as\ U_b^H U_b = I_{N_{RF}}$. By using U_b, received signal can be transformed into the beamspace.

$$y_b(t) = U_b^H y(t) = x(t) * h_b(t) + n_b(t) \in C^{N_{RF}\times 1} \quad (6)$$

where (5) is obtained by substituting (1) into (4), and

$$h_b(t) = U_b^H h(t) \in C^{N_{RF}\times 1}, \quad n_b(t) = U_b^H n(t) \in C^{N_{RF}\times 1} \quad (7)$$

Substituting equation (2) and (3) into (6) gives,

$$[h_b(t)]_s = \frac{1}{\sqrt{M}} \sum_{l=1}^{L}\sum_{m=1}^{M} \alpha_l e^{-j2\pi(m-1)(\theta_l - \bar{\theta}_{g(s)})} \times Wsinc\,[W(t-(m-1)\theta_l/f_c - \tau_l)] \quad (8)$$

where $s = 1,2,\cdots,N_{RF}$,
Fourier-transform of $n(t)$ as $\tilde{n}(f) \in C^{M\times 1}$.

Assuming that,

$$E\{\tilde{n}(f)\tilde{n}^H(f')\} = \frac{N_0}{2}\delta(f-f')I_M \quad (9)$$

The expression for received signal $y_b(t)$ in frequency domain can be written as:

$$\tilde{y}_b(f) = \tilde{x}(f)\tilde{h}_b(f) + \tilde{n}_b(f) \quad (10)$$

where $\tilde{x}(f)$ is Fourier transform of $x(t)$, and $\tilde{h}_b(f) \in C^{N_{RF}\times 1}$ is the Fourier transform of $h_b(t)$, and $\tilde{n}_b(f) \in C^{N_{RF}\times 1}$ is Fourier transform of $n_b(t)$. According to (8), we have

$$\begin{aligned}[\tilde{h}_b(f)]_s &= \frac{1}{\sqrt{M}}\sum_{l=1}^{L}\sum_{m=1}^{M} \alpha_l e^{-j2\pi(m-1)(\theta_l - \bar{\theta}_{g(s)})} \times \int_{-\infty}^{\infty} Wsinc\,[W(t-(m-1)\theta_l/f_c - \tau_l)]e^{-j2\pi ft}\,dt \\ &= \frac{1}{\sqrt{M}}\sum_{l=1}^{L}\sum_{m=1}^{M} \alpha_l e^{-j2\pi(m-1)(\check{\theta}_l(f) - \bar{\theta}_{g(s)})} e^{-j2\pi\tau_l f} \\ &= \frac{1}{\sqrt{M}}\sum_{l=1}^{L} \alpha_l e^{-j2\pi f\tau_l} G\left(\check{\theta}_l(f) - \bar{\theta}_{g(s)}\right) \times e^{j\pi(M-1)(\check{\theta}_l(f) - \bar{\theta}_{g(s)})}\end{aligned} \quad (11)$$

where $\check{\theta}_l(f) = \theta_l(f/f_c + 1)$,

International Journal of Engineering Research & Technology (IJERT)
ISSN: 2278-0181
Vol. 12 Issue 05, May-2023

$$G\left(\theta\check{}_l(f) - \theta^-_{g(s)}\right) = \frac{sin\left(\left(\theta\check{}_l(f) - \theta^-_{g(s)}\right)M\right)}{sin\left(\theta\check{}_l(f) - \theta^-_{g(s)}\right)} \quad (12)$$

According to (7), we have

$$E\{n\tilde{}_b(f)n\tilde{}_b^H(f')\} = U_b^H E\{n\tilde{}(f)n\tilde{}^H(f')\}U_b = \frac{N_0}{2}\delta(f-f')I_{N_{RF}}, \quad (13)$$

We utilize equations (9) and (3)'s orthogonality property to derive equation (13).

III. CHANNEL MODELLING

A. OFDM Symbols

To modulate the signals for transmission, OFDM symbols are utilized

$$x(t) = \sum_{n=0}^{N-1} x_n \psi_n(t) \quad (14)$$

where $x_n, n = 0,1,\cdots,N-1$ are random symbols which are independent as well, with $E\{|x_n|^2\} = E_x, \psi_n(t), n = 0,1,\cdots,N-1$ are the orthogonal waveforms given as

$$\psi_n(t) = \frac{1}{\sqrt{T}} e^{j2\pi f_n t}, 0 \le t \le T \quad (15)$$

N is the total number of subcarriers, and T is the period of the waveform. As a result, subcarriers are defined in the frequency domain as follows:

$$\psi\tilde{}_n(W,f) = \frac{e^{j2\pi(f_n - f)T} - 1}{j2\pi(f_n - f)\sqrt{T}} \quad (16)$$

where $-\frac{W}{2} \le f \le \frac{W}{2}, T = \frac{N}{W}$,
W- $x(t)$ bandwidth , f_n center frequency. Thus, the inter-subcarrier difference is $B = W/(N+1)$, and $f_n = -W/2 + nB$. So,

$$x\tilde{}(f) = \sum_{n=0}^{N-1} x_n \psi\tilde{}_n(W,f) \quad (17)$$

B. Beam Selection

Consider that we have a channel $h(t)$, according to (11), we have the frequency domain as $h\tilde{}_{ba}(f) \in C^{B\times 1}$ & the channel in the beamspace, where

$$[h\tilde{}_{ba}(f)]_n = \frac{1}{\sqrt{M}} \sum_{l=1}^{L} \alpha_l e^{-j2\pi f \tau_l} G(\theta\check{}_l(f) - \theta^-_n) \times e^{j\pi(M-1)(\theta\check{}_l(f) - \theta^-_n)} \quad (18)$$

$n = 1,2,\cdots,N$. Then, beams having largest N_{RF} values of $|[h\tilde{}_{ba}(0)]_n|$ are selected.

C. Frequency-Selective Channel Model

Consider a geometric channel model based on L scattering clusters for the frequency-selective mmWave channel [12,18]. The d-th delay touch is described in this section.

$$\mathbf{H}_d = \sum_{\ell=1}^{L} \alpha_\ell p_{\mathrm{rc}}(dT_s - \tau_\ell)\mathbf{a}_{\mathrm{R}}(\phi_\ell)\mathbf{a}_{\mathrm{T}}^*(\theta_\ell) \quad (19)$$

where $p_{\mathrm{rc}}(\tau)$ denotes raised cosine pulse signal evaluated at $\tau, \alpha_\ell \in \mathbb{C}$ is the complex gain of the ℓ th cluster, $\tau_\ell \in \mathbb{R}$ is the delay of the ℓ th cluster, ϕ_ℓ and θ_ℓ are angles of arrival and departure (AoA/AoD), respectively of the ℓ th cluster, and $\mathbf{a}_{\mathrm{R}}(\phi_\ell) \in \mathbb{C}^{N_{\mathrm{r}}\times 1}$ and $\mathbf{a}_{\mathrm{T}}(\theta_\ell) \in \mathbb{C}^{N_{\mathrm{t}}\times 1}$ denote the antenna array response vectors of receiver and transmitter, respectively.
Following is condensed channel model presented in (4):

$$\mathbf{H}_d = \mathbf{A}_{\mathrm{R}}\mathbf{\Delta}_d\mathbf{A}_{\mathrm{T}}^* \quad (20)$$

where $\mathbf{\Delta}_d \in \mathbb{C}^{L\times L}$ is diagonal with non-zero complex entries, and $\mathbf{A}_{\mathrm{R}} \in \mathbb{C}^{N_{\mathrm{r}}\times L}$ and $\mathbf{A}_{\mathrm{T}} \in \mathbb{C}^{N_{\mathrm{t}}\times L}$ contains columns $\mathbf{a}_{\mathrm{R}}(\phi_\ell)$ and $\mathbf{a}_{\mathrm{T}}(\theta_\ell)$, respectively. Under this notation, vectorizing the channel matrix in (5) gives

$$\mathrm{vec}\,(\mathbf{H}_d) = (\bar{\mathbf{A}}_{\mathrm{T}} \circ \mathbf{A}_{\mathrm{R}}) \begin{bmatrix} \alpha_1 p_{\mathrm{rc}}(dT_{\mathrm{s}} - \tau_1) \\ \alpha_2 p_{\mathrm{rc}}(dT_{\mathrm{s}} - \tau_2) \\ \vdots \\ \alpha_L p_{\mathrm{rc}}(dT_{\mathrm{s}} - \tau_L) \end{bmatrix}. \quad (21)$$

The channel from equation (6) is chosen in vector form for the subsequent sparse formulation. Important: the ℓ th column of $\bar{\mathbf{A}}_{\mathrm{T}} \circ \mathbf{A}_{\mathrm{R}}$ is formatted as $\bar{\mathbf{a}}_{\mathrm{T}}(\theta_\ell) \otimes \mathbf{a}_{\mathrm{R}}(\phi_\ell)$.

D. Sparse Formulation

Frame gearbox is improved by combining block gearbox and zero padding (ZP). To address the sparse recovery problem, we will assume that both the transmitter and receiver use a single RF chain. Nonetheless, the same strategy can be extended to include more RF chains at both ends. During the training phase, the digital precoder and combiner can be represented by the same matrices. The transmitter employs a KF precoder for the mth training frame, denoted by $\mathrm{f}_{\mathrm{RF}}^{(m)}$, which can be implemented with quantized angles at the analogue phase shifters. The next step is to obtain the nth symbol of the mth received frame.

$$\mathrm{r}_m[n] = \sum_{d=0}^{N_c-1} \mathrm{H}_d \mathrm{f}_{\mathrm{RF}}^{(m)} s_m[n-d] + \mathrm{v}_m[n] \quad (22)$$

where $s_m[n]$ represents the nth symbol in mth training frame that is non-zero

$$\mathbf{s}_m = \left[\underbrace{0\cdots 0}_{N_c-1}\, s_m[1]\cdots s_m[N]\right] \quad (23)$$

To transmit the combined signal during the m th training phase, an RF combiner $\mathrm{w}_{\mathrm{RF}}^{(m)}$ is used at the receiver. So that the post combining signal is

International Journal of Engineering Research & Technology (IJERT)
ISSN: 2278-0181
Vol. 12 Issue 05, May-2023

$$\begin{bmatrix} y_m[1] \\ y_m[2] \\ \vdots \\ y_m[N] \end{bmatrix}^T = \mathbf{w}_{\mathrm{RF}}^{(m)^*} [\mathbf{H}_0 \quad \cdots \quad \mathbf{H}_{N_c-1}] \left(\mathbf{S}_m^T \otimes \mathbf{f}_{\mathrm{RF}}^{(m)} \right) \quad (24)$$
$$+\mathbf{e}^{(m)T}$$

Where

$$\mathbf{S}_m = \begin{bmatrix} s_m[1] & 0 & \cdots & 0 \\ s_m[2] & s_m[1] & \cdots & \vdots \\ \vdots & \vdots & \ddots & \vdots \\ s_m[N] & \cdots & \cdots & s_m[N - N_c + 1] \end{bmatrix}.$$

In this scenario, block transmission with $N_c - 1$ zero padding is required because it allows for RF circuit reconfiguration between frames. It also reduces inter-frame interference and protects against training data loss during reconfiguration. It is impossible to use multiple precoders and combiners for a variety of mmWave symbols at high symbol rates. Equation (9) is the result of vectorization.

$$\mathbf{y}_m = \underbrace{\left(\mathbf{S}_m \otimes \mathbf{f}_{\mathrm{RF}}^{(m)^T} \otimes \mathbf{w}_{\mathrm{RF}}^{(m)^*} \right)}_{\boldsymbol{\Phi}_m} \begin{bmatrix} \mathrm{vec}\,(\mathbf{H}_0) \\ \mathrm{vec}\,(\mathbf{H}_1) \\ \vdots \\ \mathrm{vec}\,(\mathbf{H}_{N_c-1}) \end{bmatrix} \quad (25)$$
$$+ \mathbf{e}_m$$

IV. SIMULATION RESULTS

We conducted computer simulations and determined that an appropriate signal-to-noise ratio (SNR) for system is -10 decibels. The system consists of 256 subcarriers and has a bandwidth of 0.02 times the frequency of the carrier band, which is 60 GHz. The time delays and direction of arrivals (DOAs), or arrival angles, have a uniform distribution within the ranges [0, 2π] and [0, 256/W], respectively, where W is the number of subcarriers. There are 61 antennas distributed across the base station, and the path gain variation has been set to 1. Figure 2 compares the output response of the spectral efficiency for the Spatial-Frequency-wideband and FSCM-SF implementations at various SNR values. Our results show that FSCM-SF-based tuning yields better spectral efficiency for several reasons. Figure 3 compares the output response of the spectral efficiency and bandwidth factor, showing that the two implementations do not significantly differ in the generation of the output response. Finally, Figure 4 compares the system's spectral efficiency against the number of subcarriers. Our graph demonstrates, the Sparse Formulation of Frequency Selective Channel Model (FSCM-SF) results in an improved output response compared to the graph shown. This conclusion is supported by comparing the graphs.

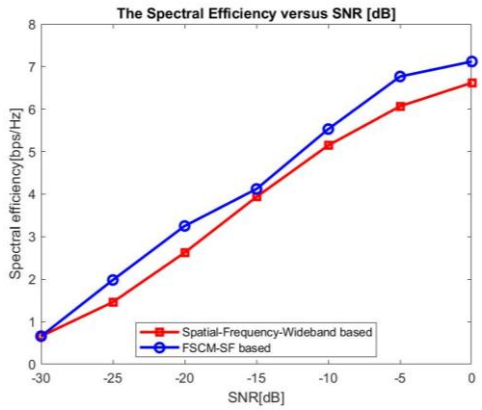

Fig 2. Comparing The Spectral Efficiency vs SNR (dB) between the Spatial-Frequency-wideband model and Frequency Selective Channel - Sparse Formulation Model

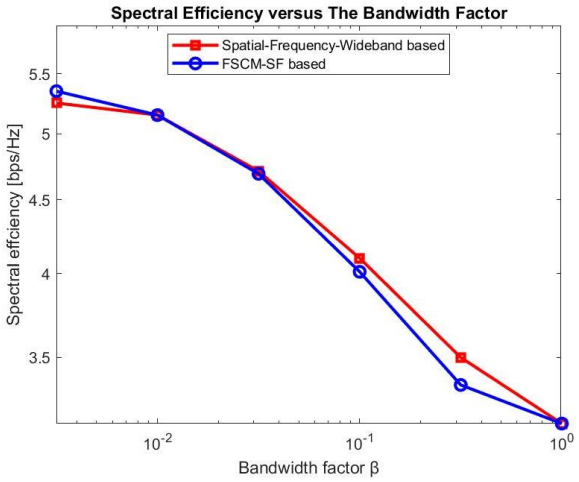

Fig 3. Comparison between Spectral Efficiency and The Bandwidth Factor (β) between the Spatial-Frequency-wideband model and Frequency Selective Channel - Sparse Formulation Model

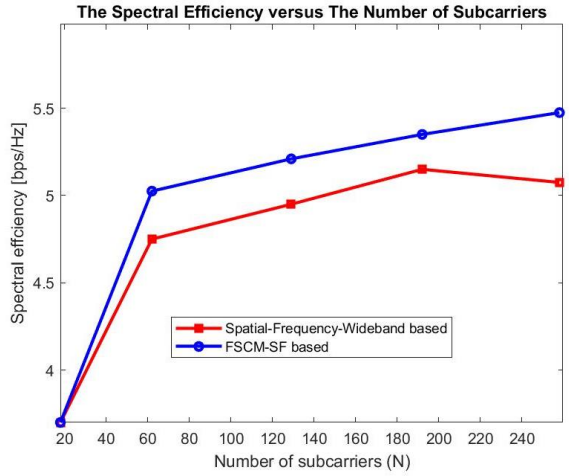

Fig 4. Comparison between the Spectral Efficiency vs The Number of Subcarriers (N) between the Spatial-Frequency-wideband model and Frequency Selective Channel - Sparse Formulation Model

International Journal of Engineering Research & Technology (IJERT)
ISSN: 2278-0181
Vol. 12 Issue 05, May-2023

V. CONCLUSION

In conclusion, the study explored the impact of wideband and hybrid receiving on the spectral efficiency of millimeter-wave OFDM uplink transmission using a frequency selective channel with sparse formulation model. The simulations showed that increasing bandwidth causes the beam squint effect to increase, which lowers spectral efficiency. The sparse formulation of the Frequency Selective Channel Model (FSCM-SF) has improved the system's spectral efficiency analysis. Simulations revealed that the FSCM-SF based implementation resulted in improved spectral efficiency compared to the Spatial-Frequency-wideband based implementation, as shown in Figure 2. Additionally, Figure 4 showed that the FSCM-SF has an improvised output response compared to the standard model. However, the system's bandwidth did not significantly affect the spectral efficiency, as shown in Figure 3. According to these findings, using a sparse formulation of the frequency selective channel model may improve the spectral efficiency of millimeter-wave OFDM uplink transmission. In order to improve system performance, this technique needs to be researched further.

REFERENCES

[1] Y. Li and A. Hu, "Wideband Millimeter-wave OFDM Uplink with Hybrid Receiving," 2021 IEEE 4th International Conference on Electronic Information and Communication Technology (ICEICT), Xi'an, China, 2021, pp. 735-739, doi: 10.1109/ICEICT53123.2021.9531323.

[2] K. -Y. Chen, H. -Y. Chang, R. Y. Chang and W. -H. Chung, "Hybrid Beamforming in mmWave MIMO-OFDM Systems via Deep Unfolding," 2022 IEEE 95th Vehicular Technology Conference: (VTC2022-Spring), Helsinki, Finland, 2022, pp. 1-7, doi: 10.1109/VTC2022-Spring 54318.2022.9860467.

[3] P. K. Korrai and D. Sen, "Performance analysis of OFDM mmWave communications with compressive sensing-based channel estimation and impulse noise suppression," 2016 IEEE International Conference on Advanced Networks and Telecommunications Systems (ANTS), Bangalore, India, 2016, pp. 1-6, doi: 10.1109/ANTS.2016.7947867.

[4] Lv, Changwei & Lin, Jia-Chin & Yang, Zhaocheng. (2019). Channel Prediction for Millimeter Wave MIMO-OFDM Communications in Rapidly Time-Varying Frequency-Selective Fading Channels. IEEE Access. PP. 1-1. 10.1109/ACCESS.2019.2893619.

[5] F. Boccardi et al, "Five disruptive technology directions for 5G," IEEE Commun. Mag., vol. 52, pp. 74-80, Feb. 2014.

[6] J. Andrews et al, "What will 5G be?," IEEE J. Sel. Areas Commun., vol. 32, pp. 1065-1082, June 2014.

[7] Z. Pi and F. Khan, "An introduction to millimeter-wave mobile broadband systems," IEEE Commun. Mag., vol. 49, pp. 101-107, June 2011.

[8] T. Rappaport et al, "Millimeter wave mobile communications for 5G cellular: It will work!," IEEE Access, vol. 1, pp. 335-349, May 2013.

[9] W. Roh et al, "Millimeter-wave beamforming as an enabling technology for 5G cellular communications: theoretical feasibility and prototype results," IEEE Commun. Mag., vol. 52, pp. 106-113, Feb 2014.

[10] A. Alkhateeb, G. Leus, and R. W. Heath, "Compressed sensing based multi-user millimeter wave systems: How many measurements are needed?,' in Proc. IEEE Int. Conf. Acoustics, Speech and Sig. Process. (ICASSP), pp. 2909-2913, April 2015.

[11] Z. Gao, L. Dai, and Z. Wang, "Channel estimation for mmwave massive MIMO based access and backhaul in ultra-dense network," in Proc. IEEE Int. Conf. on Commun. (ICC), pp. 1-6, May 2016.

[12] T. E. Bogale and L. B. Le, "Massive MIMO and mmwave for 5G wireless hetnet: Potential benefits and challenges," IEEE Veh. Technol. Mag., vol. 11, pp. 6475, March 2016.

[13] R. W. Heath, N. Gonzlez-Prelcic, S. Rangan, W. Roh, and A. M. Sayeed, "An overview of signal processing techniques for millimeter wave MIMO systems," IEEE J. Sel. Areas Commun., vol. 10, pp. 436-453, April

[14] J. Wang, "Beam codebook based beamforming protocol for multi-Gbps millimeter-wave WPAN systems," IEEE J. Sel. Areas Commun., vol. 27, pp. 1390-1399, Oct 2009.

[15] S. Hur, T. Kim, D. J. Love, J. V. Krogmeier, T. A. Thomas, and A. Ghosh, "Millimeter wave beamforming for wireless backhaul and access in small cell networks," IEEE Trans. Commun., vol. 61, pp. 4391-4403, October 2013.

[16] A. Alkhateeb, O. E. Ayach, G. Leus, and R. W. Heath Jr., "Channel estimation and hybrid precoding for millimeter wave cellular systems," IEEE J. Sel. Topics Signal Process., vol. 8, pp. 831-846, Oct 2014.

[17] R. M. Rial, C. Rusu, A. Alkhateeb, N. G. Prelcic, and R. W. Heath Jr., "Hybrid MIMO architectures for millimeter wave communications: Phase shifters or switches?," IEEE Access, Jan 2016.

[18] S. Kashyap, C. Mollen, E. Bjornson, and E. G. Larsson, "Frequency-domain interpolation of the zeroforcing matrix in massive MIMO-OFDM," in IEEE Int. Workshop Signal Process. Advances Wireless Commun. (SPAWC), pp. 1-5, July 2016.

[19] A. Alkhateeb and R. W. Heath Jr., "Frequency selective hybrid precoding for limited feedback millimeter wave systems," IEEE Trans. Commun., vol. 64, pp. 18011818 , May 2016.

[20] A. Ghosh et al, "Millimeter-wave enhanced local area systems: A high-data-rate approach for future wireless networks," IEEE J. Sel. Areas Commun., vol. 32, pp. 1152-1163, June 2014.

[21] O. E. Ayach, S. Rajagopal, S. Abu-Surra, Z. Pi, and R. W. Heath Jr., "Spatially sparse precoding in millimeter wave MIMO systems," IEEE Trans. Commun., vol. 13, pp. 1499-1513, Mar. 2014.

[22] P. Schniter and A. Sayeed, "Channel estimation and precoder design for millimeter-wave communications: The sparse way," in Proc. Asilomar Conf. Signals, Syst., Comput., pp. 273-277, Nov 2014.

[23] K. Venugopal, A. Alkhateeb, N. G. Prelcic, and R. W. Heath Jr., "Channel estimation for hybrid architecture based wideband millimeter wave systems," CoRR, vol. abs/1611.03046, 2016. http://arxiv.org/abs/1611.03046.

[24] J. Rodr´ıguez-Fern´andez and N. Gonz´alez-Prelcic, "Channel estimation for frequency-selective mmWave MIMO systems with beam-squint," in Proc.2018 IEEE Global Commun. Conf. (GLOBECOM), Abu Dhabi, United Arab Emirates, Dec. 2018, pp. 1–6,

[25] X. Gao, L. Dai, S. Zhou, A. M. Sayeed, and L. Hanzo, "Wideband beamspace channel estimation for millimeter-wave MIMO systems relying on lens antenna arrays," IEEE Trans. Signal Process., vol. 67, no. 18, pp.4809–4824, Sep. 2019.

[26] B. Wang, F. Gao, S. Jin, H. Lin, and G. Y. Li, "Spatial- and frequency wideband effects in millimeter-wave massive MIMO systems", IEEE Trans. Signal Process., vol. 66, no. 13, pp. 3393–3406, Jul. 2018.

[27] B. Wang, F. Gao, S. Jin, H. Lin, G. Y. Li, S. Sun, and T. S. Rappaport, "Spatial-wideband effect in massive MIMO with application in mmWave systems", IEEE Commun. Mag., vol. 56, no. 12, pp. 134–141, Dec. 2018.

[28] J. H. Brady and A. M. Sayeed, "Wideband communication with highdimensional arrays: New results and transceiver architectures," in Proc. 2015 IEEE Int. Conf. Commun. Workshop (ICCW), London, UK, Jun. 2015, pp. 1042–1047.

[29] A. Alkhateeb, G. Leus, and R. W. Heath, Jr., "Limited feedback hybrid precoding for multi-user millimeter wave systems," IEEE Trans. Commun., vol. 14, no. 11, pp. 6481–6494, Nov. 2015.

[30] K. Venugopal, N. Gonz´alez-Prelcic, and R. W. Heath, Jr., "Optimality of frequency flat precoding in frequency selective millimeter wave channels," IEEE Wireless Commun. Lett., vol. 6, no. 3, pp. 330–333, Jun. 2017.

[31] G. C. Ferrante, T. Q. S. Quek, and M. Z. Win, "Revisiting the capacity of noncoherent fading channels in mmWave system," IEEE Trans. Commun., vol. 65, no. 8, pp. 3259–3275, Aug. 2017.

[32] D. Zhang, Z. Zhou, C. Xu, Y. Zhang, J. Rodriguez, and T. Sato, "Capacity analysis of NOMA with mmWave massive MIMO systems," IEEE J. Sel. Areas Commun., vol. 35, no. 7, pp. 1606–1618, Jul. 2017